POLITECNICO
MILANO 1863

SCUOLA DI INGEGNERIA INDUSTRIALE
E DELL'INFORMAZIONE

Executive Summary of the Thesis

On-chip fabrication of InAs nanowires device for advanced THz detection

Laurea Magistrale in Materials Engineering and Nanotechnology - Ingegneria dei Materiali e delle Nanotecnologie

Author: Salvatore Iovinella

Advisor: Prof. Carlo Spartaco Casari

Co-advisors: Anna Fontcuberta i Morral, Valerio Piazza

Academic year: 2023-2024

1. Introduction

The terahertz (THz) is a non-ionizing radiation which shows high penetration and time resolution properties making it desirable for high-frequency optoelectronic applications. However, the lack of methods to efficiently generate and detect THz hidden this radiation in the 'Terahertz gap' for many years. The advancement of III-V technology offered interesting material platforms due to their high mobility, direct small bandgap, and short carrier life-time making them a suitable building-block for THz detection. However, bulk III-V capital cost, substrate synthesis restrictions, and high noise levels set a limitation for their use as THz detectors. III-V nanostructures are an elegant solution to reduce the material volume (hence the cost) and allow for unconventional heterostructures thanks to the relaxed requirements for lattice matching. Their high surface to volume ratio and the increased impact of high surface state density lead to properties which cannot be observed in bulk. For example, Alexander-Webber et al.[1] observed an unintuitive decrease of the photoconductivity under illumination related to H_2O and O_2 desorption and adsorption and native oxide photogating effect. They proposed atomic layer deposited (ALD) gate dielectric to reduce surface state detrimental effect. Nanowires also allow high degree of control over the photoconductive lifetime and have strong anisotropic electrical and optical properties which make them desirable for polarization sensitive detectors. For example, Peng et al.[2] demonstrated the use of vertical InP nanowires for THz full polarization state detection. InP nanowires were selected and positioned carefully in a 3D hashtag configuration. This device showed high sensitivity to the polarization state of the radiation with an almost null cross-talk. However, the photocurrent and bandwidth are limited by the active material volume. Most importantly, the pick and place method is an inefficient, non-reproducible, and non-scalable technique. In contrast, selective area epitaxy (SAE) meets the reliability and scalability requirements of industrial production. SAE is a technique that exploits a patterned dielectric mask to achieve selective growth only in specific region where the substrate is exposed. This method has been used to demonstrate horizontal InAs nanowires grown via molecular

beam epitaxy (MBE) as building block for THz detectors[3]. The devices showed also a broadband coherent detection of 3 THz. However, MBE is highly expensive and entails pattern dependent growth mechanisms. As demonstrated by Dede et al.[4], wider openings and narrower pitches show higher growth rates. Metalorganic vapour phase epitaxy (MOVPE) can overcome these limitations. Morgan et al.[5] described the growth mechanism of GaAs buffer layers with SA-MOVPE on GaAs(100) substrate. The mask was opened with trenches oriented in different directions. Along the (001) and (010) directions, the grown structures showed a triangular cross section with {101} non-polar side facets with little to no dependence on the pattern geometry. Based on the reports, SA-MOVPE appears the ideal candidate to obtain high-quality structures with geometrical and compositional control at the nanoscale.

The aim of this thesis is to investigate the fabrication of horizontal InAs nanowire (NW) devices grown by SA-MOVPE suited as THz detectors. I intend to develop both single and multi channel devices to enable polarization-sensitive detection. For this reason, the objectives of this work are: (i) fabrication of single-channel devices through metalorganic vapour phase epitaxy; (ii) definition of electrical transport in dark and impact of encapsulation; (iii) design and nano-fabrication strategies for multi-channel devices.

2. Experimental methods

This work entails the use of several cleanroom fabrication processes, epitaxial synthesis and microscopy and electrical characterization methods. A GaAs(100) 2" wafer is used as a substrate to deposit a layer of alignment markers to achieve sub-micron alignment accuracy of the subsequent layers. Markers are obtained through electron beam lithography (EBL) patterning, Cr/W bilayer sputtering, and lift-off in acetone. The surface is then prepared for SAE. A SiO_2 mask is deposited by PECVD. The nanowires pattern is transferred to the mask through EBL and reactive ion etching. The epitaxial growth is achieved with a MOVPE reactor. Once the substrate is loaded into the reactor, an annealing step is performed at 820 $°C$ for 4 min to ensure removal of the native oxide from the surface. Then a GaAs buffer (here on defined as nanomembrane, NM) is grown for 40 s at 650 $°C$. The control over the GaAs NMs allows to control the thickness and the morphology of the InAs nanowire grown for 41.6 s at 460 $°C$ subsequently on top. The nanostructures are grown along the (010) and (001) directions that allow to obtain structurally equivalent NWs [5]. The devices are completed depositing electrodes through EBL patterning, Cr/Au sputtering, and lift-off. Insulating layers are locally deposited through EBL patterning, Al_2O_3 evaporation, and lift-off. As encapsulation strategy, the final devices surface is covered by Al_2O_3 through ALD. The nanowires structural analysis is performed with secondary electron microscopy (SEM) and atomic force microscopy (AFM). Secondary transmission electron microscopy (STEM) and energy dispersive X-ray (EDX) are used for cross-sectional analysis. The devices electrical behaviour in dark conditions is studied through I-V curves, four points, and field effect measurements.

3. Single-channel THz detector

First I focused on the challenge of fabricating and characterizing horizontal InAs NWs based THz detectors through SA-MOVPE to overcome MBE limitations. Nanowires of 200 nm width are proposed in single and five array configuration with a 600 nm pitch. A structural analysis of the grown nanostructure is reported in Figure 1. The SEM and AFM data show the high regularity of the nanowires. The triangular shape cross-section formed by the presence of {101} facets is clearly visible. A small InAs parasitic growth is present on the mask due to In high sticking coefficient. This comes from local surface irregularities. In addition, an average $\sim$ 65 nm width increase from the nominal value is observed. While the parasitic growth is not expected to impact the operation of the devices, this width increase can cause major issues for complex devices reported in the next section. STEM-EDX analysis suggests lithographic overexposure as a cause for the width increase and enables to obtain data on the NWs cross section. Two samples with 20 s and 40 s InAs growth times are investigated. In both cases, the STEM micrographs show an abrupt interface between NMs and NWs. Coherently to

what demonstrated in [5], the NM shows a flat facet and {101} lateral facets. To be noted that no major morphology difference was observed in the InAs nanowires cross-section between the two samples. Nonetheless, the nanomembranes thickness was different even though the GaAs growth time was fixed to 40 s for both samples. This reveals the need for a growth time investigation to ensure the best control over the GaAs nanomembrane. The 40 s sample STEM micrograph allows to extract the cross-section area of the NWs and also showed a 55 nm increase in the opening width consistently with SEM observations. The EDX analysis confirmed no atomic inter diffusion between NMs and NWs.

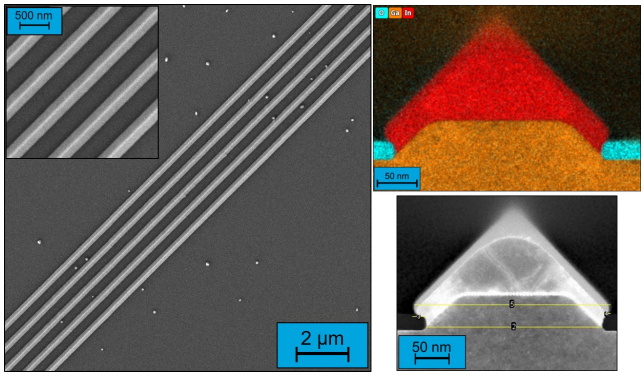

Figure 1: On the left, SEM image (with high magnification inset) of a 5-NWs array. On the right, STEM micrograph and corresponding EDX map of a nanowire cross-section.

The electrical behaviour of devices fabricated with these nanowires is characterized by current-voltage measurements in dark conditions. The single NWs showed resistances between 12 and 31 $k\Omega$, while 5NWs arrays between 4 and 9 $k\Omega$. The order of magnitude is suitable for achieving low noise levels. Four points measurements are performed on specific in-chip structures. The potential variation between the inner probes is measured as a function of the flowing current between the outer ones (Fig. 2). The resistivity is defined as:

$$\rho = R\frac{A}{s} \tag{1}$$

where R is the inner probes resistance, A is the cross-sectional area of the nanowire and s is the spacing between the inner probes. A $\rho = 3.7 \cdot 10^{-3}\Omega \cdot cm$ is found. The result is slightly lower than what is usually reported in the literature for undoped InAs NW ($0.1 - 10 \cdot 10^{-3}\Omega \cdot cm$). To be noted that the measured devices have two configurations for contacts: the "stretched" one where long nanowires run beneath the bow-tie shaped metal antennas; the "H-bar" where the nanowire(s) merge(s) with a 50 μm x 50 μm InAs thin film. The contact resistivity value found through four points measurements is $5.3 \cdot 10^{-5}\ \Omega \cdot cm^2$ corresponding to contact resistance values of the order of $0.1 - 1\ \Omega$ for the two configurations. The results demonstrated that these configurations are equivalent in terms of contact resistance.
Field effect measurements are performed on in-chip specific structures. A long nanowire represents the channel, two gold pads at the extremities are the source and the drain, and a top gated metal-oxide-semiconductor central structure works as capacitor. A voltage sweep is applied between source and drain, allowing a current to flow in the channel (I_{SD}). The gate voltage (V_G) is varied between $-5\ V$ and $5\ V$. The measured I_{SD} is plotted in function of the two voltages (Fig. 2). The mobility value is defined as:

$$\mu = \frac{\frac{\partial I_{SD}}{\partial V_G} L^2}{C_{gate} V_{SD}} \tag{2}$$

where L is the channel length, $\frac{\partial I_{SD}}{\partial V_G}$ is the slope of the I_{SD}-V_g curve for a fixed V_{SD} and C_{gate} is the capacitance estimated with parallel plate and half shell models. As both returned similar capacitance values, an average was chosen for the calculations. A $\mu = 506\frac{cm^2}{V \cdot s}$ is found. However, the mobility value for undoped InAs NW in the literature ranges from 900 to $16000\frac{cm^2}{V \cdot s}$. The causes of reduced electron mobility range from impactful defect density to unintentional NW doping during growth with C atoms of the precursors or elements present in the reactor lines. By evaluating the carrier density as:

$$n = \frac{1}{\rho \mu e} \tag{3}$$

A $n = 3.5 \cdot 10^{18} cm^{-3}$ is found, which may indicate a high level of contamination.

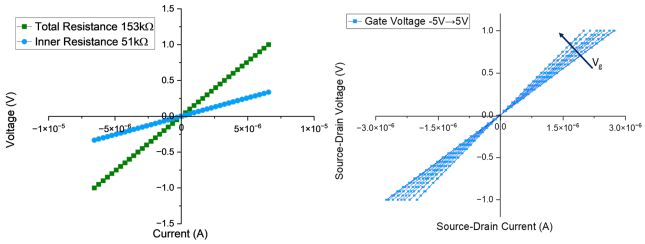

Figure 2: Current-voltage measurements: on the left 4-point measurements. On the right, field effect measurements.

Finally, an encapsulation layer strategy is explored by covering the device with an alumina layer. The impact of the encapsulation on the device performances is studied plotting the resistance variation as a function of the encapsulation thickness. Small resistance variations suggest that encapsulation does not have detrimental effects on the devices performances. The impact of encapsulation on persistent photoconductivity in InAs nanowires is studied by exposing two devices, with and without encapsulation, respectively, to a 532 nm laser and then measuring the dark resistance. An increase of resistance with illumination power and time is observed in a low dose regime. I attribute this behaviour to negative photoconductivity [1]. With high power and longer exposure time, a decreasing resistance is observed and associated with contact annealing. The latter trend is mitigated in the encapsulated device, which suggests an effective role of alumina in dispersing heat. This could be interpreted as a positive effect of alumina in reducing surface states activation.

4. Double-channel THz detector

Here I present two versions of the double-channel device designed for polarized THz detection. Having two perpendicular and equivalent channels, one can extract the polarization state as a trigonometric combination of the respective signal responses. This has been demonstrated in [2]. The two types of the device here presented differ for the channel intersection. First, I will present connected double channel devices (CDC) with semiconductor interconnect and isolated double channel devices (IDC) where the channel has metallic interconnects separated by an insulating layer. Figure 3 shows a schematic of the working principle.

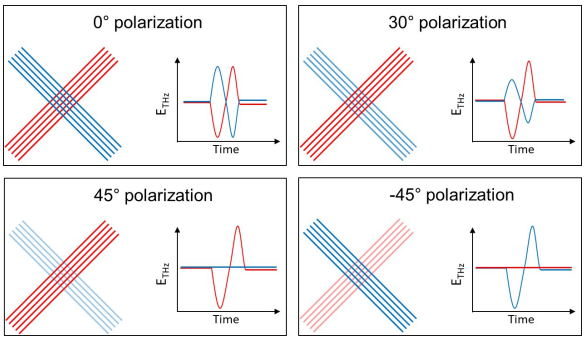

Figure 3: Polarization detection working principle. Each channel signal intensity is proportional to the polarization state.

4.1. CDC device

The CDC device consists of superimposed (010) and (001) oriented NWs connected in the central area. The structural analysis allows to understand the effect of the design parameters on the epitaxial growth. Structures with pitches of 500, 600, and 700 nm are grown and analysed at SEM. The nanowires appear to be regular, although different morphologies could be observed between the centre and the outer regions of the device. The first shows a flat (100) facet predominance. The latter presents the triangular shape cross section. Samples with different InAs growth times (20 s and 40 s) show a flat central area. The height profile acquired with AFM along the nanowires length reports staircase-like features. Reference [5] demonstrated how wider openings require longer growth time to complete the NW triangular cross-section. This suggests that the cause of the flattening is probably EBL overexposure. Samples with a half nominal width (100 nm) show a two-fold increase in width but also a dramatic reduction of flattening, which is confined in the very centre of the cross points. Overall, these evidences indicate that EBL parameters fine tuning can counter the issue.

The electrical behaviour in dark condition of the CDC devices is studied through current-voltage measurements. The I-V curves extracted across each pair of antennas show similar resistance values and are plotted together in Figure 4. The result suggests that the nanostructures are perfectly equivalent and regular in all directions, creating a highly symmetric system. However,

this also means that cross-talking occurs between channels, which is not optimal for polarization detection. Interestingly, CDC devices show higher resistances values with respect to single-channel devices in equivalent configuration (Fig. 4). The source of this difference could be related to the crystal quality at the intersection where additional defects can arise. The encapsulation thickness test for CDC devices shows random oscillations of resistance variation consistently with the results on single channel devices. The alumina layer seems to not have any effect on the system symmetry -i.e. on the cross-talk.

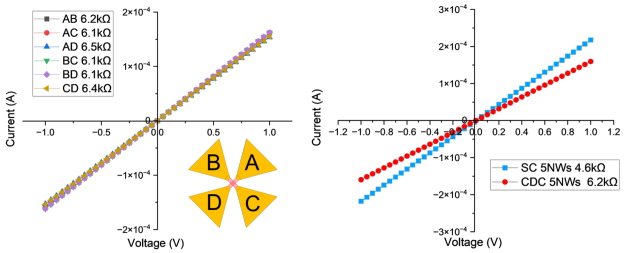

Figure 4: I-V curves for each antenna pair of CDC device (left) and a comparison with SC device (right)

4.2. IDC device

The isolated double channel (IDC) device is developed to overcome the cross-talk issue of the CDC device. In this design, the perpendicular nanowires are grown intersection-free, leaving a gap in the centre of the device. Isolated metallic bridges are used to electrically contact the sub-channels. The micro-scale dimensions of the central elements add a high degree of complexity to the fabrication. The metallic bridges and the oxide square used for isolation need to be accurately deposited in a 4 x 4 μm window. EBL is able to achieve precision on the order of tens of nanometres. The lateral resolution can be pushed below $\sim$ 100 nm, but it requires several calibration tests. In addition, the overexposure effect can easily cause a short circuit between the metallic elements, and hence a fine tuning of the parameters set is needed to achieve the highest accuracy.

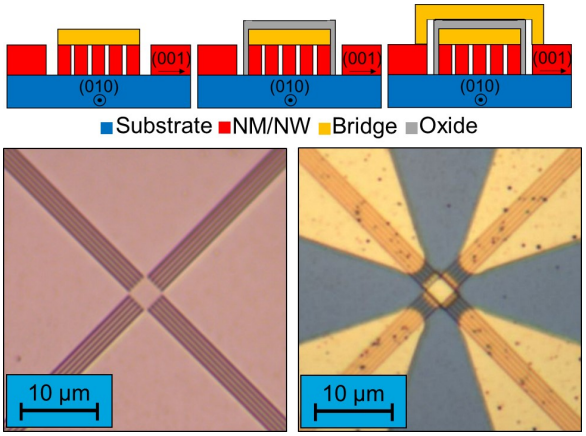

Figure 5: Bridging fabrication steps on top. Optical images comparison between substrate state after growth (left) and after fabrication (right).

The first big challenge encountered is related, indeed, to bridge misalignment which caused short-circuits of the channels. To be noted that devices on the same chip experience different direction shifts. The reason is found in the alignment system. The CAMP are markers used to establish a reference system for the lithography tool. The common three CAMP system is sensible to rotation errors. If one of the marker positions is slightly shifted, the angle between the x and y axis will not perfectly correspond to 90°. This causes a precision error in the writing which is enhanced as the feature is smaller and farther from the origin of the system. The issue was solved by implementing a five CAMP alignment system. The first CAMP is used with the second and third to define a first reference system. The fourth and fifth CAMP are used to correct the defined coordinates. The new alignment algorithm allows to achieve high accuracy. The oxide deposition did not present relevant issues. The second bridge instead showed delamination problems. After deposition, because of the complex morphology of the central area, the bridge probably resulted in contact with the sacrificial layer. Consequently, during the lift-off, all the metal film is removed. This issue was tackled by thickening the electron resist to increase the height distance between the bridge and the sacrificial layer. The enhanced alignment system, processing accuracy, and geometrical parameters tuning allow for the fabrication of perfectly aligned IDC devices. Figure 5 reports a comparison between the as grow nanostructures and the device final fabrication state.

The IDC devices are electrically tested through I-V curves. However, a current spike is immediately observed at low voltages. Optical and SEM analyses reveal several damages to the top bridge, oxide square, and nanowires. The cause is attributed to a charge accumulation at the dielectric interfaces. Considering the size of the central bridges and the cross-sectional area of the nanowires, it is reasonable to expect that the central area works as a capacitor and the charges are instantaneously released upon voltage application, burning the devices. A new design model is proposed to protect the device. The antennas are connected during the lithography step in order to favour charge redistribution in the whole device. Then, right before the current voltage measurements, the connections are broken to isolate again the channels.

5. Conclusions

Several advancements are made on defining a reproducible and scalable fabrication method for SA-MOVPE grown horizontal InAs nanowires for polarized THz detection.
First, single-channel devices are investigated. The SEM and AFM analyses reveal high regularity of the nanowires topography but also larger width. The STEM analysis allows to extract NW cross-sectional data and associate the cause of width increase to EBL overexposure. STEM-EDX excludes interdiffusion between GaAs NM and InAs NW. Current-voltage measurements reveal resistance values in the order of $k\Omega$. The found resistivity value agrees with bibliographic standards. The mobility and carrier concentration values suggest possible unintentional doping of the NWs during growth. The encapsulation strategy shows promising preliminary results.
Second, double-channel detector designs are proposed. The CDC shows a morphological variation along the NW length. AFM and SEM analyses allow to attribute this feature to EBL overexposure. Smaller widths solve the issue. The I-V curves show the high symmetry of the structures although this reveals cross-talking between channels. This probably also explains the highest resistance measured with respect to SC devices. The encapsulation test shares the results found for SC devices. The IDC device fabrication presents different challenges to tackle such as misalignment and delamination. Five CAMP system and parameters fine-tuning are employed to finally achieve perfectly aligned devices. The IDC detectors seem to accumulate charges in the central area, causing catastrophic release and damage during measurements. A grounding strategy is suggested to favour charges redistribution.

6. Acknowledgements

I want to thank my advisors Carlo Casari, Anna Fontcuberta i Morral and Valerio Piazza for giving me this opportunity and for their precious counsel.
I want to acknowledge Michele Zendrini for his valuable contribution in the epitaxial growth process. Claire Blaga for her help with the encapsulation test under illumination. Lucie Navratilova and Victor Boureau for their amazing work in lamellas preparation and STEM analysis.
Special thanks to all the LMSC members who contributed with their amusing mood and interesting ideas.

References

[1] Jack A. Alexander-Webber and al. Engineering the photoresponse of inas nanowires. *ACS Applied Materials & Interfaces*, 9(50):43993–44000, 2017. PMID: 29171260.

[2] Kun Peng and al. Three-dimensional cross-nanowire networks recover full terahertz state. *Science*, 2020.

[3] Nicholas Morgan and al. Direct and integrating sampling in terahertz receivers from wafer-scalable inas nanowires. *Nature communications*, 2023.

[4] Didem Dede and al. Selective area epitaxy of gaas: the unintuitive role of feature size and pitch. *Nanotechnology*, 33(48):485604, sep 2022.

[5] Nicholas Morgan and al. From layer-by-layer growth to nanoridge formation: Selective area epitaxy of gaas by movpe. *Crystal Growth and Design*, 2023.